FEBS Letters 583 (2009) 835–840

FEBS Letters

journal homepage: www.FEBSLetters.org

Conformational changes in p47^{phox} upon activation highlighted by mass spectrometry coupled to hydrogen/deuterium exchange and limited proteolysis

Julien Marcoux [a,b,c,d], Petr Man [b,c,d,1], Mathieu Castellan [a,c,d], Corinne Vivès [a,c,d], Eric Forest [b,c,d,*], Franck Fieschi [a,c,d,*]

[a] Laboratoire des Protéines Membranaires, CEA, DSV, Institut de Biologie Structurale (IBS), 41 rue Jules Horowitz, Grenoble F-38027, France
[b] Laboratoire de Spectrométrie de Masse des Protéines, CEA, DSV, Institut de Biologie Structurale (IBS), 41 rue Jules Horowitz, Grenoble F-38027, France
[c] CNRS, UMR 5075, Grenoble, France
[d] Université Joseph Fourier, Grenoble, France

ARTICLE INFO

Article history:
Received 19 December 2008
Revised 21 January 2009
Accepted 23 January 2009
Available online 2 February 2009

Edited by Miguel De la Rosa

Keywords:
NADPH oxidase
p47^{phox}
H/D exchange
Limited proteolysis
Conformational change

ABSTRACT

The neutrophil NADPH oxidase is an enzymatic complex involved in innate immunity. Phosphorylation of p47^{phox} promotes its translocation with p67^{phox} and p40^{phox}, followed by membrane interaction and assembly with flavocytochrome b_{558} into a functional complex. To characterise p47^{phox} conformational changes during activation, we used wild-type and the S303/304/328E triple mutant mimicking the phosphorylated state. Hydrogen/deuterium exchange and limited proteolysis coupled to mass spectrometry were used to discriminate between the various structural models. An increase in deuteration confirmed that p47^{phox} adopts an open and more flexible conformation after activation. Limited proteolysis correlated this change with increased auto-inhibitory region (AIR) accessibility. These results establish a structural link between the AIR release and the exposure of the Phox homology (PX) domain.

1. Introduction

The neutrophil NADPH oxidase complex has been widely studied over the past 30 years [1]. This multi-component complex is the archetype for a recently expanded group of enzymes divided into seven families named on the basis of the membranal redox component: Nox1, Nox2, Nox3, Nox4, Nox5, Duox1 and Duox2 [2,3]. They are found in many cellular types and play different physiological roles, for instance in microbicidal activity, hormone synthesis and vascular tone control [3]. The neutrophil NADPH oxidase complex (based on Nox2) is one of the first barriers during the nonspecific immune response. Its main role is the destruction of phagocytosed pathogens through the superoxide anion $O_2^{\cdot-}$. The reactive oxygen is produced by the oxidase complex in neutrophilic vacuoles by transferring electrons from the NADPH donor to molecular oxygen. The importance of this complex is illustrated by the occurrence of chronic granulomatous disease (CGD) upon mutation(s) of one of its components.

The overall assembly process of this membranal complex has already been thoroughly studied [1,4]. However, its activation and regulation still need to be clearly elucidated. The catalytic core of the NADPH oxidase complex is represented by flavocytochrome b_{558}. It enables electron transfer and is composed of two membrane proteins, Nox2 and p22^{phox}. The other parts of the complex are cytosolic proteins: p40^{phox}, p67^{phox}, p47^{phox} and Rac(1 or 2), a small G protein. Except for Rac, these proteins undergo phosphorylations during the NADPH oxidase activation [5,6]. Upon phosphorylation, all cytosolic factors translocate to the membrane-bound catalytic core, which triggers the activation of the whole assembly.

Due to their modular nature, p40^{phox}, p67^{phox} and p47^{phox} have been reluctant to crystallisation trials and X-ray structure determination. Finally, the structure of the entire p40^{phox} has been recently released [7], while the structures of the entire p67^{phox} and p47^{phox} remain unknown. Therefore, structural and functional studies on these two proteins have long been conducted using their isolated

Abbreviations: ACN, acetonitrile; phox, phagocyte oxidase; AIR, autoinhibitory region; SH_3, src homology 3; PX, Phox homology; SAXS, small-angle X-ray scattering; GST, glutathione *S*-transferase; DTT, 1-4, dithiothreitol; PtdIns(3,4)P_2, phosphoinositol-3,4-biphosphate; SDS, sodium dodecyl sulfate; PAGE, polyacrylamide gel electrophoresis; ESI, electrospray ionization; TOF, time of flight.

* Corresponding authors. Address: Institut de Biologie Structurale (IBS), 41 rue Jules Horowitz, Grenoble F-38027, France. Fax: +33 4 38 78 54 94 (F. Fieschi).
E-mail addresses: eric.forest@ibs.fr (E. Forest), franck.fieschi@ibs.fr (F. Fieschi).
[1] Present address: Institute of Microbiology, Academy of Sciences of the Czech Republic, v.v.i, CZ-14220 Prague 4, Czech Republic.

0014-5793/$34.00
doi:10.1016/j.febslet.2009.01.046

modules [8–14]. Indeed, p47^{phox} has been investigated to determine whether it plays a role as a complex organiser triggered by its activation. Based on structural data obtained with isolated modules, a model for the activation of p47^{phox} was proposed [6,10,15]. According to these studies, p47^{phox} exists as an auto-inhibited form in the resting state. The auto-inhibition state has been explained by intramolecular interactions between the Phox homology (PX) domain and the $SH3_B$ [16,17] and between the tandem SH3s and an auto-inhibiting region (AIR) [9,12,18]. During activation, these modules are believed to be unmasked, enabling PX domain interaction with membrane anionic phospholipids [10,19] and the tandem SH3s interaction with the p22^{phox} C-terminus [13,14]. However, this model seems unlikely because the second $SH3_B$ cannot interact with the PX and the AIR at the same time, since both partners would use the same binding site [9,17].

Our group recently presented a revised model based on small-angle X-ray scattering (SAXS) studies of the entire protein, showing that the p47^{phox} auto-inhibited form was more elongated than expected [20]. This new model suggests that the AIR binds to the tandem SH3s and proposes a new interaction mode for the PX domain with both $SH3_A$ and the AIR. At this stage, additional data are required to confirm and refine the details of the auto-inhibited model but also to describe the molecular rearrangements occurring upon p47^{phox} activation.

In this study, we used wild-type auto-inhibited p47^{phox} and a triple mutant (S303/304/328E) known to mimic the phosphorylated activated form of p47^{phox} [9,10,15,21,22]. Using H/D exchange coupled to mass spectrometry, we followed solvent accessibility and flexibility modifications occurring upon conformational changes from the resting to the activated state. In addition, limited proteolysis identified modifications in the AIR's susceptibility to cleavage. Based on the results presented herein, we established a structural link between the simultaneous releases of the AIR and PX in a p47^{phox} construct integrating all the functional modules involved in the activation process.

2. Materials and methods

2.1. Materials

Glutathione Sepharose high-performance and SP Sepharose high-performance columns came from GE Healthcare. The Jupiter 5 μm C18 column (50 × 1.00 mm; 300 Å) was from Phenomenex. Protein MacroTrap (C8) was purchased from Michrom Bioresources.

The following products were purchased from Avanti Polar Lipids: 1-palmitoyl-2-oleyl-*sn*-glycero-3-phosphocholine (POPC), 1-palmitoyl-2-oleyl-*sn*-glycero-3-phosphoethanolamine (POPE), 1-palmitoyl-2-oleyl-*sn*-glycero-3-phosphate (POPA) and 1,2-dioleoyl-*sn*-glycero-3-[phosphoinositol-3,4-biphosphate] (PtdIns (3, 4)P_2).

2.2. p47^{phox} cloning, expression and purification

cDNA encoding p47^{phox} residues 1–342 was cloned into pGex-6P vector adding an N-terminal glutathione *S*-transferase (GST) fusion tag. After GST cleavage, 10 additional residues remained at the N-terminus of the protein. These additional residues will be referred to as negative numbers in peptide numbering and the resulting p47^{phox} (−10–342) construct as p47^{phox}ΔCter. The triple mutation S303/304/328E was introduced by PCR-mediated site-directed mutagenesis, leading to the form mimicking the activated p47^{phox}, referred to as p47^{phox}TM-ΔCter. The proteins were expressed in *Escherichia coli* BL21(DE3) and purified according to Durand et al. [20].

2.3. Binding the PX domain to multi-lamellar vesicles (MLV)

The in vitro semi-quantitative liposome-binding assay was adapted from Ago et al. [16] with minor modifications. Liposomes were prepared by mixing POPC and POPE (50:50) for the control (MLV1) and POPC, POPE, POPA and PtdIns(3,4)P_2 (45:45:5:5) for specific liposomes (MLV2). The mixture was then dried under nitrogen and resuspended to a concentration of 2 mM of total lipids in a binding buffer (20 mM Tris, pH 7.4, 100 mM NaCl, 1 mM 1-4, dithiothreitol (DTT)). After 2 h of incubation on ice, liposomes were obtained by vortexing. Proteins (5 μM) were incubated with liposomes (1 mM) for 15 min at 20 °C in 100 μL binding buffer. Liposomes were collected by ultracentrifugation (45 min at 49 000 rpm in a TLA 100.4 rotor) and aliquots were taken for further analysis by 12% sodium dodecyl sulfate–polyacrylamide gel electrophoresis (SDS–PAGE). Coomassie Blue-stained gels were scanned and analysed by densitometry. Three independent experiments were conducted.

2.4. Limited proteolysis analysis

Chymotrypsin and trypsin were chosen among other proteases (elastase, thermolysin) by SDS–PAGE digestion pattern screening. Aliquots (5 μg/well) were taken at 15 min, 30 min, 1 h, 2 h and 3 h and the different protein/enzyme ratios were analysed. p47^{phox} incubation with 0.5‰ chymotrypsin or trypsin at 20 °C displayed significant differences between p47^{phox}ΔCter and p47^{phox}TM-ΔCter digestion patterns (Fig. 3).

The p47^{phox} digests were loaded onto a Protein MacroTrap and desalted with 0.03% TFA for 1 min. The peptides were eluted on a C18 column and separated by a three-step elution (5 min at 35% acetonitrile (ACN), 10 min at 45% ACN and 2 min at 100% ACN). The column was directly interfaced to an ESI-TOF-MS (Agilent). The most representative digestion times were reported here (1 h and 3 h for trypsin and chymotrypsin, respectively). The masses of detected peptides were searched for against the p47^{phox} sequence using the FindPept software.

2.5. Global H/D exchange kinetics

The exchange of p47^{phox}ΔCter and p47^{phox}TM-ΔCter was initiated by a 20-fold dilution in a deuterated buffer (5 mM HEPES, pD 7.4, 1 mM EDTA, 2 mM DTT and 200 mM NaCl). Aliquots (40 μl) were taken after 10 s, 30 s, 1 min, 5 min, 10 min, 30 min, 1 h, 3 h, 5 h, 7 h and 9 h. The exchange was quenched by adding 5.6 μL of 50 mM HCl and rapid freezing in liquid nitrogen. Next, each sample was quickly thawed, online desalted on Protein MacroTrap, eluted with 70% ACN and analysed using ESI-TOF-MS. The spectra were smoothed and deconvoluted with Magtran software [23]. Deuteration levels were calculated according to Zhang and Smith [24]. Three independent measurements were taken.

3. Results and discussion

3.1. p47^{phox}ΔCter and p47^{phox}TM-ΔCter are representative of the resting and activated states of full-length p47^{phox}

Conformational changes that occur during p47^{phox} phosphorylation promote new interactions with membrane lipids and p22^{phox} membrane protein [10,14,19]. The PX domain, the tandem SH3s and the AIR are directly involved in these interaction property changes. On the contrary, the C-terminal region of p47^{phox} (343–390) is only required for p67^{phox} and p40^{phox} interaction, allowing their co-translocation to the membrane [25,26]. In addition, this C-terminal region of p47^{phox} is not involved in binding

to p22^{phox} [9,18] or to PI(3,4)P_2 lipids [27]. The full-length recombinant form of p47^{phox} is well expressed but is unstable due to the high protease sensitivity of its C-terminal region during purification. Therefore, to avoid heterogeneity of the sample, a C-terminal truncated form of p47^{phox} (p47^{phox}ΔCter) was used. It contains all the structural elements involved in the locking of p47^{phox} in its resting state. Using NMR and CD spectroscopy, Shen et al. [27] have recently demonstrated that such C-terminal truncation does not induce global or domain unfolding.

It was previously shown that mutations of serines 303, 304 and 328 into glutamates were sufficient to mimic their phosphorylation and the transition from a resting to an activated state. These mutated forms were shown to bind membranes and p22^{phox} with a greater affinity than p47^{phox} [10,15,16]. Moreover, they induce the $O_2^{\cdot-}$ production by the whole NADPH oxidase complex [21]. The truncated triple mutant S303/304/328E, p47^{phox}TM-ΔCter, was generated as a model of activated p47^{phox}. The existence of two distinct conformations, with increased flexibility in the activated state, has been suggested to account for the interaction with the membrane [15]. To confirm this hypothesis and demonstrate the functionality of the construct, p47^{phox}ΔCter and p47^{phox}TM-ΔCter were first incubated with nonspecific and specific liposomes, with BSA as a negative control. As expected, none of the proteins bound to nonspecific vesicles (MLV1, bound/unbound <0.5); BSA did not interact with any vesicles (Fig. 1). In contrast, both p47^{phox}ΔCter and p47^{phox}TM-ΔCter interacted with liposomes containing 5% PI(3,4)P_2 (MLV2), but at different levels. Interestingly, the weak interaction of p47^{phox}ΔCter shows that the autoinhibited conformation is not locked as tightly as has often been suggested. This basal interaction of the p47^{phox}ΔCter form with lipids was also observed in similar pull-down experiments and suggests an equilibrium between two different conformations (closed and open) [10,16,27]. Interaction was greater for p47^{phox}TM-ΔCter (bound/unbound = 14.7 ± 0.2) than for the p47^{phox}ΔCter (bound/unbound = 6.4 ± 0.6). This stronger interaction between p47^{phox}TM-ΔCter and MLV2 clearly shows its activated conformation. The membrane-binding ratio increase for the activated state of p47^{phox} agrees with previous reports by other groups [10,16], confirming that the mutations introduced favor a more open conformation and increased access to the PX module.

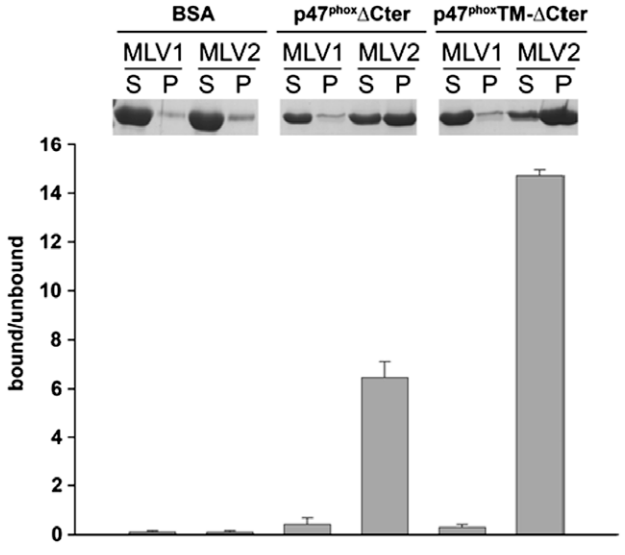

Fig. 1. Phosphoinositide-binding activity of p47^{phox}ΔCter and p47^{phox}TM-ΔCter vs negative control, BSA. p47^{phox}ΔCter, p47^{phox}TM-ΔCter or BSA were incubated with liposomes containing POPC:POPE 50:50 (MLV1) or POPC:POPE:POPA:PtdIns(3,4)P2 45:45:5:5 (MLV2). S and P are liposomal supernatant and pellet after centrifugation, corresponding to the unbound and bound fraction, respectively. Samples were analysed by SDS–PAGE and quantified by densitometry.

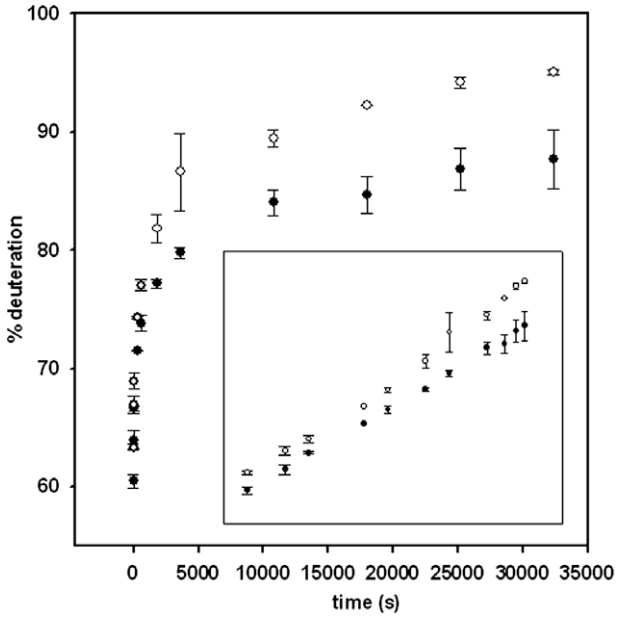

Fig. 2. Deuteration kinetics for p47^{phox}ΔCter (●) and p47^{phox}TM-ΔCter (○) at pD 7.4. The inset is a replot of the curves on the logarithmic scale.

3.2. The activated state of p47^{phox} presents an increased solvent accessible surface and flexibility

Until now, the activated state of the entire p47^{phox} has been defined as an open state, as demonstrated by functional studies [15]. Indeed, the structural data obtained so far have always been determined on isolated modules leading to inconsistent sets of data regarding the locking mechanism of the entire protein, as described previously [20]. To structurally describe the potential conformational events occurring in the whole protein upon activation, we followed the time course of deuteration for both p47^{phox} forms. This technique is today widely used to better characterise non-

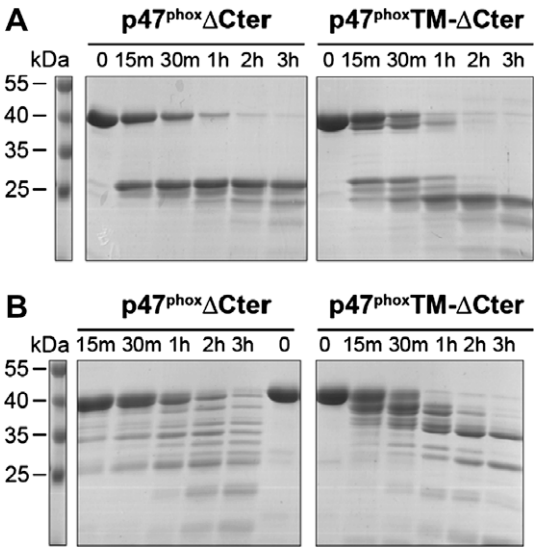

Fig. 3. SDS–PAGE of p47^{phox}ΔCter and p47^{phox}TM-ΔCter proteolysis with 0.5‰ chymotrypsin (A) and trypsin (B).

crystallizing protein and protein dynamics or interactions [24,28,29]. The deuteration kinetics showed a significant difference between p47^{phox}ΔCter and p47^{phox}TM-ΔCter proteins (Fig. 2). Higher deuteration levels of p47^{phox}TM-ΔCter that are already visible after few seconds of exchange (inset, Fig. 2) could be interpreted as "opening" the protein, resulting in an increase in the surface exposed to the solvent. The steady increase in the difference between p47^{phox}ΔCter and p47^{phox}TM-ΔCter may also point to another change: higher structural flexibility of the activated form. These global deuteration kinetics are the first experimental evidence of structural differences between the auto-inhibited and activated forms of p47^{phox}.

3.3. Upon activation, the AIR goes from a hindered to an exposed state

Local information on structural differences can be obtained by limited proteolysis, as is commonly used for protein domain determination [30]. The digestion time course was followed with 0.5‰ trypsin or chymotrypsin. Aliquots were collected at the times indicated above and all samples were resolved on SDS–PAGE (Fig. 3). Direct visual inspection of Coomassie Blue-stained gels clearly showed lower molecular-weight bands for p47^{phox}TM-ΔCter than for p47^{phox}ΔCter, reflecting better protease accessibility and suggesting a more open and/or flexible conformation for the activated form. LC-ESI-TOF analysis of p47^{phox}ΔCter digested with 0.5‰ chymotrypsin supported these findings by identifying the two major masses corresponding to the −10–139 and 140–342 peptides (Fig. 4A). However, more than two peaks were obtained after digestion of p47^{phox}TM-ΔCter (Fig. 4B). Two major peaks again corresponded to the −10–139 and 140–342 peptides while other peaks matched the −10–324, −10–331, 140–324 and 140–331 peptides. Trypsin limited proteolysis (0.5‰) generated more peptides than chymotrypsin after 1 h (see supplementary data). We identified 19 peaks for each protein (Table 1) generated through 12 cleavage sites. From the trypsin and chymotrypsin digests, four common cleavage sites were identified: Arg_{85}, Tyr_{139}, Lys_{143} and Lys_{146}. We also found specific cleavage sites after $Arg_{335/336/337}$ for p47^{phox}ΔCter and after $Arg_{292/296/314/316/318}$, Lys_{295}, Tyr_{324} and Phe_{331} for p47^{phox}TM-ΔCter.

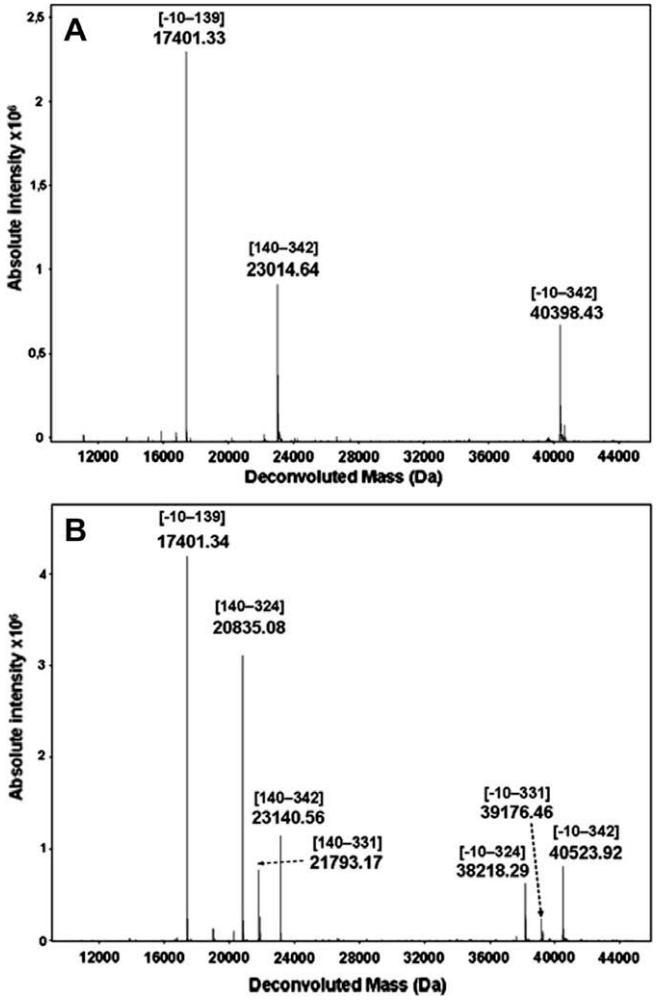

Fig. 4. Deconvoluted ESI-TOF mass spectra of p47^{phox}ΔCter (A) and p47^{phox}TM-ΔCter (B) after 3 h of digestion with chymotrypsin at 0.5‰. Annotations show first and last amino acids of each peptide detected.

These common sites are easily explained by our model. Tyrosine 139 and lysines 143 and 146 are situated in a linker region between the PX domain and the SH_3 tandem expected to be unstructured and highly flexible (Fig. 5) [20]. However, this region has recently been suggested to be involved in the activation process and more precisely to play an active role in maintaining the auto-inhibited conformation [27]. If different structural states of this linker exist in both p47^{phox} forms, this approach cannot discriminate them. The fourth common site, Arg_{85}, is located at the beginning of a loop linking two helices in the PX structure [10], whereas the other lysines and arginines from PX belong to secondary structure elements. Thus, only Arg_{85} is accessible by trypsin in the PX domain. The existence of this cleavage site in both p47^{phox} forms suggests that this side of the PX is always accessible and probably not involved in a locking interaction in the auto-inhibited form.

The specific cleavage sites, $Arg_{335,336,337}$, are situated in the flexible C-terminal part of p47^{phox} downstream of the AIR, which

Table 1
Identified peptides after digestion of p47^{phox}ΔCter and p47^{phox}TM-ΔCter with 0.5‰ trypsin or chymotrypsin (experimental masses and mass errors are given).

Limited proteolysis							
p47^{phox}ΔCter				p47^{phox}TM-ΔCter			
Exp. mass	Sequence			Exp. mass	Sequence		
	From	To	ppm		From	To	ppm
Trypsin							
40399.7	−10	342	−17	37541.54	−10	318	−13
39890.03	−10	337	−14	37257.74	−10	316	−21
39733.58	−10	336	−8	37014.65	−10	314	−22
39577.42	−10	335	−8	36604.66	1	318	99
39462.68	1	342	−17	36320.65	1	316	−14
38952.92	1	337	−12	36077.41	1	314	−23
38796.05	1	336	5	34908.12	−10	296	−20
38640.62	1	335	−14	34752.1	−10	295	−27
28700.65	86	337	−7	34382.76	−10	292	−22
28388.28	86	335	−7	33971.29	1	296	−21
21736.55	147	337	−53	33445.46	1	292	−17
21723.05	144	335	13	18860.38	147	314	−25
21422.84	147	335	8	18172.36	−10	146	−16
18172.33	−10	146	−12	17872.17	−10	143	−23
17872.19	−10	143	−20	17235.43	1	146	−24
17235.48	1	146	−19	16934.87	1	143	−9
16934.9	1	143	−12	16228.42	147	292	−20
11206.87	−10	85	1	11206.88	−10	85	9
10270.31	1	85	−31	10270.56	1	85	−59
Chymotrypsin							
40398.43	−10	342	15	40523.92	−10	342	30
23014.64	140	342	12	39176.46	−10	331	29
17402.33	−10	139	−12	38218.29	−10	324	32
				23140.56	140	331	20
				21793.17	140	342	14
				20835.08	140	324	15
				17401.34	−10	139	45

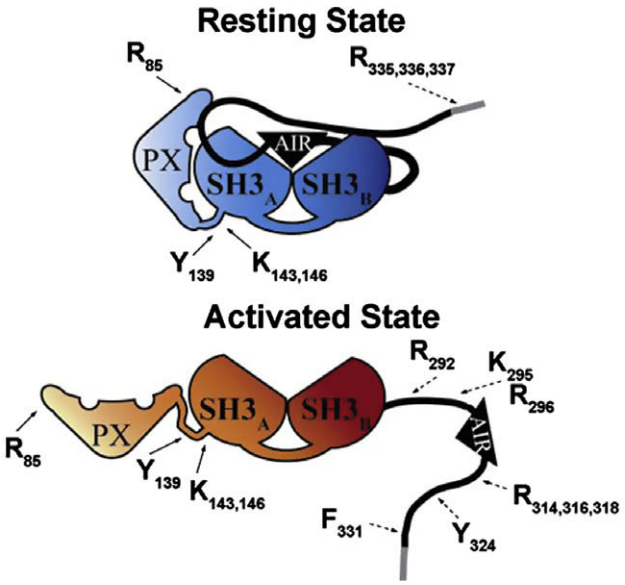

Fig. 5. Schematic representation of the cleavage sites obtained after digestion with 0.5‰ trypsin and chymotrypsin. Common sites are represented with solid arrows and specific sites for p47^{phox}ΔCter and p47^{phox}TM-ΔCter with dashed arrows. AIR, auto-inhibiting region (represented in black).

explains their accessibility in p47^{phox}ΔCter. Peptides generated by these cleavage sites in p47^{phox}ΔCter, such as 1–335, 1–336 and 1–337, are not present when digesting the p47^{phox}TM-ΔCter because the tryptic proteolysis went further and generated shorter peptides, such as 1–316, 1–314 or 1–292. Moreover, all eight specific cleavage sites ($Arg_{292/296/314/316/318}$, Lys_{295}, Tyr_{324} and Phe_{331}) of p47^{phox}TM-ΔCter are part of the AIR. This domain was shown to be implicated in the auto-inhibition of tandem SH3s [9] and we confirm here that it is more accessible and flexible in the p47^{phox}TM-ΔCter activated state.

3.4. Conclusion and perspectives

This study compared two conformational states of p47^{phox} that play a key role in the activation process of the neutrophil NADPH oxidase. The global H/D exchange kinetics revealed a significant difference in deuteration between the two constructs, which can be interpreted as an increase in both solvent accessibility and structural flexibility of the activated form. This was further supported by limited proteolysis of p47^{phox}ΔCter and p47^{phox}TM-ΔCter, identifying eight extra cleavage sites in the AIR of p47^{phox}TM-ΔCter. To our knowledge, this work is the first structural approach on a p47^{phox} form integrating all the modules involved in its auto-inhibition. It confirms the existence of conformational changes between the inhibited and activated forms. We demonstrated that incorporation of negative charges in positions 303, 304 and 328 results in the release of the AIR from a hindered to an accessible state. This confirms that the AIR and the tandem SH3s form a super-complex in auto-inhibited p47^{phox}, as has previously been hypothesised from structural analysis on isolated domains [9]. Furthermore, enhancement of the PX–lipid interaction is associated with the AIR release, confirming the need for a well-constituted "tandem SH3s-AIR super-complex" for PX locking. From our previously described SAXS-derived envelope of the entire p47^{phox}, the PX domain can only fit laterally to this "tandem SH3s-AIR super-complex" in the auto-inhibited state [20]. Altogether, this suggests that there are contacts between the PX and parts of this super-complex (Fig. 5). This model is in full agreement with the behaviour of the W263R mutation in the tandem SH3s, as previously described [10]. This mutation is an alternate way to generate a lipid-binding activated state of p47^{phox}. Indeed, in this mutant, exaltation of the PX properties may result from the initial disruption of the "tandem SH3s–AIR super-complex". In accordance with this view, a recent in vivo study has contributed new data arguing in favor of this type of organisation [22].

A complete characterisation of the p47^{phox} auto-inhibitory organisation would require the identification of an interaction interface between the PX domain and the $SH3_A$ domain and/or loop(s) within the AIR. The difference observed during global deuteration kinetics opens the way to local hydrogen/deuterium exchange kinetics so that the spatial resolution of these results can be increased considerably [24,28,29]. This approach is particularly well suited to identifying such interfaces and is currently underway.

Appendix A. Supplementary data

Supplementary data associated with this article can be found, in the online version, at doi:10.1016/j.febslet.2009.01.046.

References

[1] Vignais, P.V. (2002) The superoxide-generating NADPH oxidase: structural aspects and activation mechanism. Cell Mol. Life Sci. 59, 1428–1459.
[2] Lambeth, J.D. (2004) NOX enzymes and the biology of reactive oxygen. Nat. Rev. Immunol. 4, 181–189.
[3] Nauseef, W.M. (2008) Biological roles for the NOX family NADPH oxidases. J. Biol. Chem. 283, 16961–16965.
[4] Li, X.J., Fieschi, F., Paclet, M.H., Grunwald, D., Campion, Y., Gaudin, P., Morel, F. and Stasia, M.J. (2007) Leu505 of Nox2 is crucial for optimal p67phox-dependent activation of the flavocytochrome *b*558 during phagocytic NADPH oxidase assembly. J. Leukoc. Biol. 81, 238–249.
[5] el Benna, J., Faust, L.P. and Babior, B.M. (1994) The phosphorylation of the respiratory burst oxidase component p47phox during neutrophil activation. Phosphorylation of sites recognized by protein kinase C and by proline-directed kinases. J. Biol. Chem. 269, 23431–23436.
[6] Massenet, C., Chenavas, S., Cohen-Addad, C., Dagher, M.C., Brandolin, G., Pebay-Peyroula, E. and Fieschi, F. (2005) Effects of p47phox C terminus phosphorylations on binding interactions with p40phox and p67phox. Structural and functional comparison of p40phox and p67phox SH3 domains. J. Biol. Chem. 280, 13752–13761.
[7] Honbou, K., Minakami, R., Yuzawa, S., Takeya, R., Suzuki, N.N., Kamakura, S., Sumimoto, H. and Inagaki, F. (2007) Full-length p40phox structure suggests a basis for regulation mechanism of its membrane binding. EMBO J. 26, 1176–1186.
[8] Grizot, S., Fieschi, F., Dagher, M.C. and Pebay-Peyroula, E. (2001) The active N-terminal region of p67phox. Structure at 1.8 A resolution and biochemical characterizations of the A128V mutant implicated in chronic granulomatous disease. J. Biol. Chem. 276, 21627–21631.
[9] Groemping, Y., Lapouge, K., Smerdon, S.J. and Rittinger, K. (2003) Molecular basis of phosphorylation-induced activation of the NADPH oxidase. Cell 113, 343–355.
[10] Karathanassis, D., Stahelin, R.V., Bravo, J., Perisic, O., Pacold, C.M., Cho, W. and Williams, R.L. (2002) Binding of the PX domain of p47(phox) to phosphatidylinositol 3, 4-bisphosphate and phosphatidic acid is masked by an intramolecular interaction. EMBO J. 21, 5057–5068.
[11] Taylor, R.M. et al. (2007) Characterization of surface structure and p47phox SH3 domain-mediated conformational changes for human neutrophil flavocytochrome *b*. Biochemistry 46, 14291–14304.
[12] Yuzawa, S., Ogura, K., Horiuchi, M., Suzuki, N.N., Fujioka, Y., Kataoka, M., Sumimoto, H. and Inagaki, F. (2004) Solution structure of the tandem Src homology 3 domains of p47phox in an autoinhibited form. J. Biol. Chem. 279, 29752–29760.
[13] Nobuhisa, I., Takeya, R., Ogura, K., Ueno, N., Kohda, D., Inagaki, F. and Sumimoto, H. (2006) Activation of the superoxide-producing phagocyte NADPH oxidase requires co-operation between the tandem SH3 domains of p47phox in recognition of a polyproline type II helix and an adjacent alpha-helix of p22phox. Biochem. J. 396, 183–192.
[14] Ogura, K., Nobuhisa, I., Yuzawa, S., Takeya, R., Torikai, S., Saikawa, K., Sumimoto, H. and Inagaki, F. (2006) NMR solution structure of the tandem Src homology 3 domains of p47phox complexed with a p22phox-derived proline-rich peptide. J. Biol. Chem. 281, 3660–3668.
[15] Ago, T., Nunoi, H., Ito, T. and Sumimoto, H. (1999) Mechanism for phosphorylation-induced activation of the phagocyte NADPH oxidase protein p47(phox). Triple replacement of serines 303, 304, and 328 with aspartates disrupts the SH3 domain-mediated intramolecular interaction in p47(phox), thereby activating the oxidase. J. Biol. Chem. 274, 33644–33653.
[16] Ago, T., Kuribayashi, F., Hiroaki, H., Takeya, R., Ito, T., Kohda, D. and Sumimoto, H. (2003) Phosphorylation of p47phox directs phox homology domain from

SH3 domain toward phosphoinositides, leading to phagocyte NADPH oxidase activation. Proc. Natl. Acad. Sci. USA 100, 4474–4479.
[17] Hiroaki, H., Ago, T., Ito, T., Sumimoto, H. and Kohda, D. (2001) Solution structure of the PX domain, a target of the SH3 domain. Nat. Struct. Biol. 8, 526–530.
[18] Yuzawa, S., Suzuki, N.N., Fujioka, Y., Ogura, K., Sumimoto, H. and Inagaki, F. (2004) A molecular mechanism for autoinhibition of the tandem SH3 domains of p47phox, the regulatory subunit of the phagocyte NADPH oxidase. Genes Cells 9, 443–456.
[19] Ago, T., Takeya, R., Hiroaki, H., Kuribayashi, F., Ito, T., Kohda, D. and Sumimoto, H. (2001) The PX domain as a novel phosphoinositide- binding module. Biochem. Biophys. Res. Commun. 287, 733–738.
[20] Durand, D., Cannella, D., Dubosclard, V., Pebay-Peyroula, E., Vachette, P. and Fieschi, F. (2006) Small-angle X-ray scattering reveals an extended organization for the autoinhibitory resting state of the p47(phox) modular protein. Biochemistry 45, 7185–7193.
[21] Inanami, O., Johnson, J.L. and Babior, B.M. (1998) The leukocyte NADPH oxidase subunit p47PHOX: the role of the cysteine residues. Arch. Biochem. Biophys. 350, 36–40.
[22] Ueyama, T. et al. (2008) Sequential binding of cytosolic Phox complex to phagosomes through regulated adaptor proteins: evaluation using the novel monomeric Kusabira–Green System and live imaging of phagocytosis. J. Immunol. 181, 629–640.
[23] Zhang, Z. and Marshall, A.G. (1998) A universal algorithm for fast and automated charge state deconvolution of electrospray mass-to-charge ratio spectra. J. Am. Soc. Mass Spectrom. 9, 225–233.
[24] Zhang, Z. and Smith, D.L. (1993) Determination of amide hydrogen exchange by mass spectrometry: a new tool for protein structure elucidation. Protein Sci. 2, 522–531.
[25] Dusi, S., Donini, M. and Rossi, F. (1996) Mechanisms of NADPH oxidase activation: translocation of p40phox Rac1 and Rac2 from the cytosol to the membranes in human neutrophils lacking p47phox or p67phox. Biochem. J. 314 (Pt 2), 409–412.
[26] Heyworth, P.G., Curnutte, J.T., Nauseef, W.M., Volpp, B.D., Pearson, D.W., Rosen, H. and Clark, R.A. (1991) Neutrophil nicotinamide adenine dinucleotide phosphate oxidase assembly. Translocation of p47-phox and p67-phox requires interaction between p47-phox and cytochrome b558. J. Clin. Invest. 87, 352–356.
[27] Shen, K., Sergeant, S., Hantgan, R.R., McPhail, L.C. and Horita, D.A. (2008) Mutations in the PX-SH3A linker of p47phox decouple PI(3, 4)P2 binding from NADPH oxidase activation. Biochemistry 47, 8855–8865.
[28] Brier, S., Lemaire, D., Debonis, S., Forest, E. and Kozielski, F. (2004) Identification of the protein binding region of S-trityl-L-cysteine, a new potent inhibitor of the mitotic kinesin Eg5. Biochemistry 43, 13072–13082.
[29] Man, P., Montagner, C., Vernier, G., Dublet, B., Chenal, A., Forest, E. and Forge, V. (2007) Defining the interacting regions between apomyoglobin and lipid membrane by hydrogen/deuterium exchange coupled to mass spectrometry. J. Mol. Biol. 368, 464–472.
[30] Gao, X. et al. (2005) High-throughput limited proteolysis/mass spectrometry for protein domain elucidation. J. Struct. Funct. Genomics 6, 129–134.